Topological Effects on Intramolecular Electron Transfer via Quantum Interference

Cendrine Patoux, Christophe Coudret, Jean-Pierre Launay,* Christian Joachim,* and André Gourdon

Molecular Electronics Group, Centre d'Elaboration de Matériaux et d'Etudes Structurales, UPR 8011, CNRS, 29 rue Jeanne Marvig, 31055 Toulouse Cedex, France

Received January 8, 1997[⊗]

The three isomers of diferrocenylbenzenes (ortho, **1o**; meta, **1m**; para, **1p**) as well as 5-substituted derivatives of *m*-diferrocenylbenzene with R = NH_2 (**2**), Cl (**3**), CH_3 (**4**), CN (**5**), NO_2 (**6**), and $N(CH_3)_3^{3+}$ (**7**) have been prepared. Crystal structures of **1o**, **3**, and **5** have been solved. In **3** and **5**, the cyclopentadienyl rings are nearly parallel to the benzene mean planes with angles ranging from 9.99(5)° to 14.74(5)°. One ferrocene group is above and the other below the mean molecular plane. For **1o**, there is an important twist between the benzene and cyclopentadiene rings (68.6(8)° and 32.5(8)°) for steric reasons. Controlled potential electrolysis yields the mixed-valence ferrocene/ferrocenium species in comproportionation equilibrium with homovalent species. Intervalence transitions have been observed and corrected from comproportionation. From the intervalence band parameters, metal−metal couplings (V_{ab}) are calculated using Hush's equation. The values are much higher for **1o** (0.025 eV) and **1p** (0.043 eV) than for **1m** (0.012 eV) and exhibit little or no variation for the substituted *m*-diferrocenylbenzenes **2**−**6**. These results are rationalized by extended Hückel molecular orbital calculations. The weakness of the interaction in **1m** can be ultimately traced to a quantum Interference effect, i.e., a cancellation of the contributions of two electron transfer paths. This cancellation occurs because each path implies a mixing of metal orbitals with a different ligand orbital, and the resulting molecular orbitals exhibit different symmetries.

Introduction

Intramolecular electron transfer can be monitored by the study of intervalence transitions occurring in mixed-valence complexes.[1] In the frame of a general study about electron transfer and molecular switching,[2−4] we have been interested in determining the factors responsible for the interaction between two metal atoms connected through a bridging ligand. This interaction is currently characterized by the V_{ab} parameter, which has the dimension of an energy, and corresponds to the effective coupling between metal localized orbitals. V_{ab} can be obtained from the position, intensity, and width of the intervalence transition which occurs generally in the near infrared.[1,5]

Interesting behaviors can be expected when the V_{ab} coupling is small as a result of cancellation effects, because one could expect a great sensitivity to small perturbations. This could be the basis of a switching process based on *quantum interference*. In fact, such effects have been foreshadowed in the literature. Thus in 1983, Richardson and Taube[6] reported the marked difference in behavior between ruthenium complexes bridged by either 1,3-dicyanobenzene or 1,4-dicyanobenzene (i.e., meta *vs* para isomers). A weak V_{ab} coupling occurred in the former with respect to the latter, and more generally, when the substituent position was changed systematically, an "alternation effect was found, which was expected on the basis of general experience with the transmission of electronic effects through conjugated bond systems".[6] In the same spirit, Hunter *et al.* have found a stronger interaction for para-disubsituted organometallic complexes than for meta isomers,[7] although these authors focus mainly on the wave splitting $\Delta E_{1/2}$ (equivalent to $\Delta E°$) between the redox processes associated with the two sites.[8]

In 1993, we described the peculiar properties of the 2,7,9,-10-tetraazaphenanthrene ligand for which the V_{ab} coupling is lower than would be predicted from simple superposition rules based on the topology of the ligand.[9] This showed that adding a new branch in a given ligand does not necessarily increase the coupling, a fact reminiscent of the classical properties of

[⊗] Abstract published in *Advance ACS Abstracts,* October 1, 1997.

(1) See, for instance, the reviews by Crutchley and Creutz: Crutchley R. J. *Adv. Inorg. Chem.* **1994**, *41*, 273−325. Creutz, C. *Prog. Inorg. Chem.* **1983**, *30*, 1−73. Some recent examples: Benniston, A. C.; Goulle, V.; Harriman, A.; Lehn, J.-M.; Marczinke, B. *J. Phys. Chem.* **1994**, *98*, 7798−7804. Haga, M.-a.; Ali, Md. M.; Koseki, S.; Fujimoto, K.; Yoshimura, A.; Nozaki, K.; Ohno, T.; Nakajima, K.; Stufkens, D. J. *Inorg. Chem.* **1996**, *35*, 3335−3347. Elliot, M. E.; Derr, D. L.; Ferrere, S.; Newton, M. D.; Liu, Y.-P. *J. Am. Chem. Soc.* **1996**, *118*, 5221−5228.

(2) Collin, J.-P.; Lainé, P.; Launay, J.-P.; Sauvage, J.-P.; Sour, A. *J. Chem. Soc., Chem. Commun.* **1993**, 434−435. Beley, M.; Chodorowski-Kimmes, S.; Collin, J.-P.; Lainé, P.; Launay, J.-P.; Sauvage, J.-P. *Angew. Chem., Int. Ed. Engl.* **1994**, *33*, 1775−1778. Lainé, P.; Marvaud, V.; Gourdon, A.; Launay, J.-P.; Argazzi, R.; Bignozzi, C.-A. *Inorg. Chem.* **1996**, *35*, 711−714.

(3) Ribou, A.-C.; Launay, J.-P.; Takahashi, K.; Nihira, T.; Tarutani, S.; Spangler, C. W. *Inorg. Chem.* **1994**, *33*, 1325−1329.

(4) Ribou, A.-C.; Launay, J.-P.; Sachtleben, M. L.; Li, H.; Spangler, C. W. *Inorg. Chem.* **1996**, *35*, 3735−3740.

(5) Hush, N. S. *Prog. Inorg. Chem.* **1967**, *8*, 391−444. Hush, N. S. *Coord. Chem. Rev.* **1985**, *64*, 135−157.

(6) Richardson, D. E.; Taube, H. *J. Am. Chem. Soc.* **1983**, *105*, 40−51.

(7) Chukwu, R.; Hunter, A. D.; Santarsiero, B. D.; Bott, S. G.; Atwood, J. L.; Chassaignac, J. *Organometallics* **1992**, *11*, 589−597.

(8) The "electronic interaction" is frequently loosely assimilated with the wave splitting $\Delta E_{1/2}$ (equal to $\Delta E°$) which occurs when a molecule containing two equivalent redox sites exhibits two oxidation or reduction waves. Although $\Delta E°$ and V_{ab} may depend on the same parameters and may exhibit parallel variations, they represent different types of interaction. V_{ab} is truly a measure of the indirect interaction of the metal orbitals mediated by the bridging ligands in the mixed-valence complex. For most of the compounds investigated here it is a through-bond coupling. $\Delta E°$ is a thermodynamic quantity involving not only the mixed-valence species under investigation but also the homovalent species associated in the redox equations. It measures the additional difficulty to reduce (or oxidize) a given site when its neighbor already has been reduced (or oxidized). $\Delta E°$ depends on V_{ab} but also on other factors, for instance the through-space distance between metal sites and the effective dielectric constant of the medium.[27] The present paper is mainly devoted to the study of V_{ab} couplings.

(9) Marvaud, V.; Launay, J.-P.; Joachim, C. *Chem. Phys.* **1993**, *177*, 23−30.

S0020-1669(97)00013-X CCC: $14.00

Scheme 1

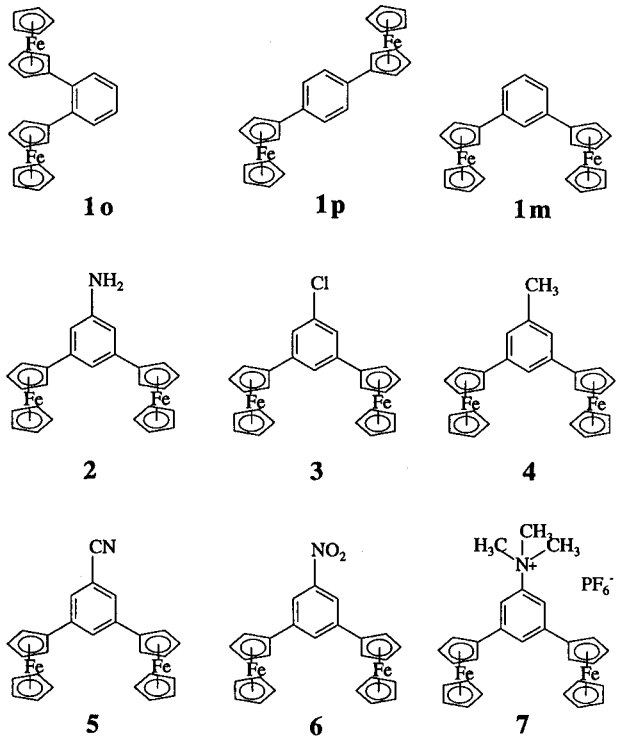

interferometric devices. This was attributed to the existence of two coupling channels with different symmetry properties. A related effect has been theoretically studied by Ratner *et al.*, who showed that inclusion of non-nearest-neighbor interactions (which is equivalent to adding a new coupling channel) changes the pattern of resonance and interference effects.[10]

The influence of several parallel electron transfer paths also has been studied by Beratan *et al.*[11] in the case of protein electron transport. Finally, in recent years, Paddon-Row *et al.*[12] have shown that topological interference can explain the peculiar electron transfer properties of polynorbornyl bridges. A detailed analysis based on the parity rule (couplings are algebraic quantities with alternating + and − signs when the number of relays on a given pathway increases) shows that destructive interference may occur when there is "crosstalk" between two parallel paths. Although their analysis concerns specifically coupling through σ bonds, it bears similarity to the present problem where π couplings are involved.

We have thus undertaken an experimental and theoretical study of the effect of topology on intramolecular electron transfer. The studied compounds contain ferrocene groups, which proved convenient for the spectroscopic detection of weak interactions in the mixed-valence state.[4] In addition, the chemistry of ferrocene is well-known and versatile enough to yield a large variety of products.

In the present paper, we first describe intervalence transitions and V_{ab} couplings in diferrocenylbenzenes with ortho, meta, and para connection (compounds **1o**, **1m**, **1p**, Scheme 1). This allows a preliminary study of the influence of topology on electron transfer. Then, starting from the structure of *m*-diferrocenylbenzene (**1m**), we study the influence of a third

Scheme 2

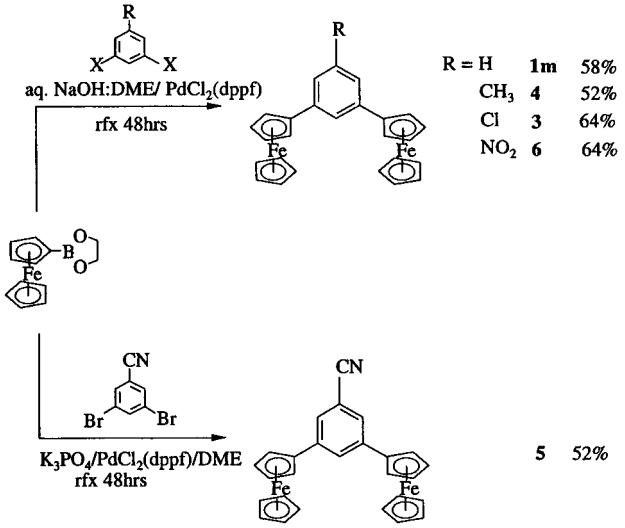

group R introduced in the 5-position, giving **2** (R = NH_2), **3** (R = Cl), **4** (R = CH_3), **5** (R = CN), **6** (R = NO_2), and **7** (R = $N(CH_3)_3^{3+}$), this list being arranged more or less in the order of increasing Hammet parameters, i.e., from strong donors to strong acceptors.

The results are then interpreted in the frame of molecular orbitals via a four-level model. After identification of the specific molecular orbitals of the bridging unit which determine the coupling, we show that a cancellation happens, which explains the weakness of the couplings in meta isomers. This observation is in agreement with a destructive interference effect occurring during the charge transfer process through the meta isomer ligand. The conditions to observe this quantum interference effect are developed.

Results and Discussion

1. Syntheses. Since poor results were obtained by the Bachmann−Gomberg−Hay[13] reaction between ferrocene and phenylenetetrazonium salts,[14] a longer route, involving an aromatic, palladium-catalyzed cross-coupling reaction, was selected.

A first approach was to react dihalobenzenes with ferrocenylzinc chloride, in the presence of $Pd(PPh_3)_4$ (i.e., Negishi's conditions[15]). Good results were obtained for the *p*-diferrocenylbenzene (**1p**), but the reaction failed for the ortho (**1o**) and meta (**1m**) isomers. Difficulties in scaling up the preparation of monobromoferrocene[16] precursor of the organozinc reagent free of 1,1′-disubstituted ferrocene prompted us to look for another method.

The air-stable[17] ferrocenylboronic acid, conveniently prepared in one step from ferrocene,[18] is a suitable reagent for the Suzuki

(10) Cheong, A.; Roitberg, A. E.; Mujica, V.; Ratner, M. A. *J. Photochem. Photobiol. A: Chem.* **1994**, *82*, 81−86.
(11) Regan, J. J.; Risser, S. M.; Beratan, D. N.; Onuchic, J. N. *J. Phys. Chem.* **1993**, *97*, 13083−13088 and references therein.
(12) Shephard, M. J.; Paddon-Row, M. N.; Jordan, K. D. *J. Am. Chem. Soc.* **1994**, *116*, 5328−5333. Shephard, M. J.; Paddon-Row, M. N. *J. Phys. Chem.* **1995**, *99*, 17497.
(13) (a) Little, W. F.; Reilley, C. N.; Johnson, J. D.; Lynn, K. N.; Sanders, A. P. *J. Am. Chem. Soc.* **1964**, *86*, 1376−1381, (b) 1382−1386. (c) Little, W. F.; Nielsen, B.; Williams, R. *Chem. Ind.* **1964**, 195. (d) Roe, A.; Little, W. F. *J. Org. Chem.* **1955**, *20*, 1577−1590.
(14) Schoutissen, H. A. J. *J. Am. Chem. Soc.* **1933**, *55*, 4531−4534.
(15) Lee, M. T.; Foxman, B. M.; Rosenblum, M. *Organometallics* **1985**, *4*, 539−547. Chambron, J.-C.; Coudret, C.; Sauvage, J.-P. *New J. Chem.* **1992**, *16*, 361−367. Negishi, E. I.; Takahashi, T.; King, A. O. In *Organic Syntheses*; Freeman, J. P., Ed.; John Wiley: New York, 1993; Collect. Vol. 8, pp 430−434.
(16) Fish, R. W.; Rosenblum, M. *J. Org. Chem.* **1965**, *30*, 1253−1254.
(17) Upon standing, ferrocenylboronic acid is slowly converted into an insoluble material. Esterification with diols is a well-known procedure to stabilize boronic acids without changing their reactivity in Suzuki's cross-coupling reaction.[20].
(18) Sawamura, M.; Sasaki, H.; Nakata, T.; Ito, Y. *Bull. Chem. Soc. Jpn.* **1993**, *66*, 2725−2729.

Scheme 3

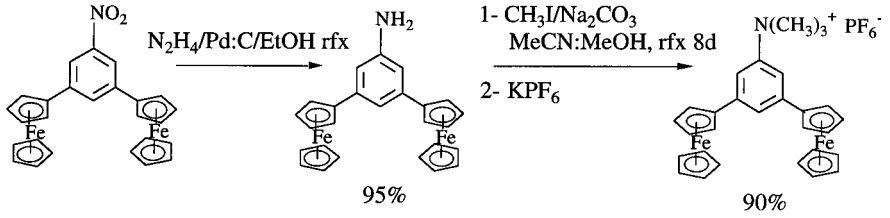

6 **2** **7**

aromatic cross coupling, in a DME/aqueous NaOH mixture, using $PdCl_2$(dppf) as catalyst, as shown by Rehahn *et al.*[19] Four new diferrocenylbenzenes have been obtained by reacting this ester with various dihalobenzenes (Scheme 2). The reaction proceeds well for the electron deficient dibromobenzenes, giving the chloro (**3**) or nitro (**6**) derivatives in 64% yield, and its efficiency is only slightly decreased for the electron rich 3,5-dibromotoluene: the methyl derivative **4** is obtained in 52% yield. Even the sterically hindered *o*-diiodobenzene reacts under these conditions, and the previously unknown *o*-diferrocenylbenzene (**1o**) has been obtained, albeit in poor yield (8%). However, this strongly basic aqueous reaction mixture is not suitable for readily hydrolyzable substituents, and the preparation of the cyano derivative **5** required anhydrous conditions such as those developed by Suzuki.[20] By using K_3PO_4 as the base in dry DME, we have been able to obtain compound **5** in 52% yield. Non commercially available 1,3-dibromobenzenes were prepared by bromination of the appropriate aniline (4-aminobenzonitrile) followed by reductive deamination (4-amino-3,5-dibromobenzonitrile, 2,6-dibromo-4-nitroaniline, and 2,6-dibromo-4-chlorobenzene) using standard procedures.[21]

Once the ferrocene group has been introduced into the molecular framework, classic functional group interconversion reactions such as the almost quantitative NO_2 reduction by hydrazine[22] and amine permethylation [23] have been used to prepare compounds bearing the electron-donating amino group (**2**) or the electron-withdrawing trimethylammonium group (**7**) (Scheme 3).

All of the new diferrocenylbenzenes have been thoroughly characterized by standard techniques. As expected, ^{1}H-NMR spectra show that protons on the benzene ring are sensitive to the electron-withdrawing influence of the substituent on the 5-position of the ring, leading to an increase of their chemical shifts. This effect is weakly transmitted to the ferrocenyl groups. A typical charge transfer absorption of the arylferrocene chromophore[24] around 450 nm is observed for all compounds and is remarkably independent of the 5-substituent. Mass spectrometry shows the expected fragmentation of ferrocenyl derivatives, that is, a successive loss of cyclopentadienyl and iron.

2. Crystal and Molecular Structures of 1o, 3, and 5. The molecular structures in the solid state of **1o**, **3**, and **5** have been established by single-crystal X-ray diffraction analyses. Crystallographic data and parameters for structure refinements are given in Table 1, while selected bond lengths and torsion angles are given in Table 2. Figures 1, 2, and 3 show respectively **1o**, **3**, and one of the two molecules of the asymmetric unit of **5** at a probability level of 30%.

Table 1. Crystallographic Data for and Refinement Parameters of **1o**, **3**, and **5**

	1o	**3**	**5**
formula	$C_{26}H_{22}Fe_2$	$C_{26}H_{21}Fe_2Cl$	$C_{27}H_{21}Fe_2N$
fw (g mol^{-1})	446.16	480.60	471.16
space group	*Pcab*	$P2_1/n$	$P\bar{1}$
temp (°C)	24	24	24
a (Å)	9.426(1)	14.92(1)	12.702(1)
b (Å)	9.909(1)	8.022(3)	13.389(1)
c (Å)	41.87(1)	17.40(1)	14.330(1)
α (deg)	90	90	109.50(1)
β (deg)	90	97.59(5)	90.77(1)
γ (deg)	90	90	113.37(1)
V (Å^3)	3911(1)	2065(2)	2078(4)
Z	8	4	4
F(000)	1840	984	968
cryst size (mm)	0.8, 0.2, 0.2	0.4, 0.4, 0.1	0.8, 0.7, 0.3
λ (Å)	0.71069	0.71069	0.71069
μ(MoK$_\alpha$) (cm^{-1})	1.49	1.55	1.41
ρ_{calcd} (g cm^{-3})	1.52	1.55	1.51
no. of unique reflns	3421	3571	5901
no. of obsd reflns	1409	2863	4080
weighting scheme	Chebyshev	unit	unit
R^a	0.059	0.037	0.042
$R_w{}^b$	0.052	0.040	0.047
resd dens (e/Å^3)	−0.7, +0.69	−0.38, +0.52	−0.79, +0.45

^{a} $R = \sum||F_o| - |F_c||/\sum|F_o|$. ^{b} $R_w = [\sum w(|F_o| - |F_c|)^2/\sum w|F_o|^2]^{1/2}$.

In **3** and **5**, one ferrocene group is above and the other below the mean molecular plane. The cyclopentadienyl rings are nearly parallel to the benzene mean planes with angles ranging from 9.99(5)° to 14.74(5)°. In contrast, the steric constraints between the two ferrocene units in the ortho derivative **1o**, and in particular between H(24) and C(10), C(11), and C(14) (distances 2.619(8), 2.872(8), and 2.756(8) Å, respectively), increase the twist angles between the benzene ring and the cyclopentadiene rings (68.6(8)° and 32.5(8)°). This steric repulsion has no effect on the planarity of the phenyl ring itself, but maintains C(10) 0.151(5) Å above the benzene ring, whereas C(20) is slightly below this ring by 0.037(5) Å, with a torsion angle C(10)−C(100)−C(101)−C(20) of 7.55(8)°. In all three compounds, the interannular C(Cp)−C(phenyl) distances (1.466(8)−1.49(1) Å) are identical within experimental errors, which indicates little influence of conjugation between the aromatic rings. An important conjugation between the nearly coplanar electron-releasing ferrocenyl group and the electron-withdrawing benzonitrile part in **5** would have shortened the C(Cp)−C(phenyl) bond in comparison with the more perpendicular conformation in **1o**.[25]

(19) Knapp, R.; Rehahn, M. *J. Organomet. Chem.* **1993**, *452*, 235−240.
(20) Watanabe, T.; Miyaura, N., Suzuki, A. *Synlett* **1992**, 207−210.
(21) Furniss, B. S.; Hannaford, A. J.; Smith, P. W. G.; Tatchell, A. R. *Vogel's Textbook of Practical Organic Chemistry*, 5th ed.; Longman Scientific & Technical: Harlow, 1989; pp 909 and 943−944.
(22) Sessler, J. L.; Mody, T. D.; Ramasamy, R.; Sherry, A. D. *New J. Chem.* **1992**, *16*, 541−544.
(23) Sandler, S. R.; Karo, W. *Organic Functional Group Preparations*, 2nd ed.; Academic Press: London, 1983; Vol. 1, p 386.
(24) Toma, S.; Gaplovsky, A.; Hudecek, M.; Langfelderova, Z. *Monatsh. Chem.* **1985**, *116*, 357−364.
(25) See, for example: Roberts, M. G.; Silver, J.; Yamin, B. M.; Drew, M. G. B.; Eberhardt, U. *J. Chem. Soc., Dalton Trans.* **1988**, 1549−1556.

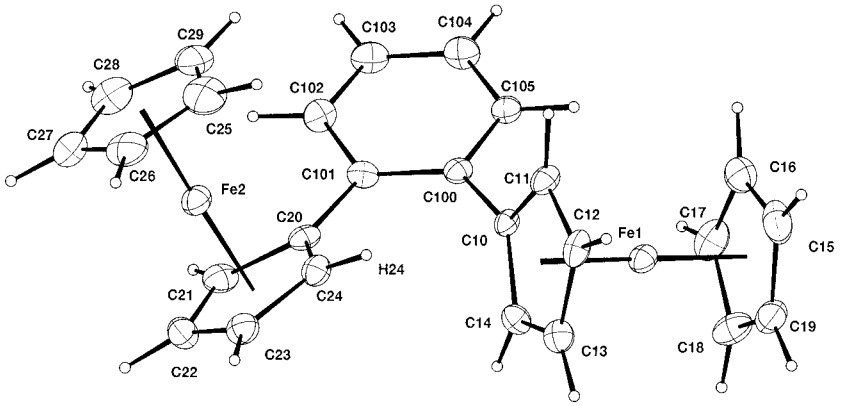

Figure 1. Molecular structure of **1o**.

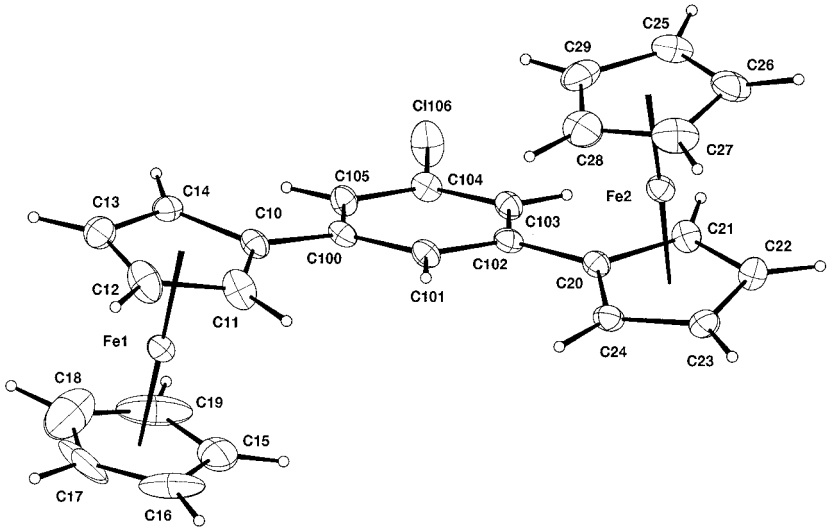

Figure 2. Molecular structure of **3**.

Table 2. Selected Bond Lengths and Torsion Angles

		Interannular C(Cp)−C(phenyl) Bond Distances (Å)		
1o	C(10)−C(100)	1.49(1)	C(20)−C(101)	1.48(1)
3	C(10)−C(100)	1.471(5)	C(20)−C(102)	1.468(5)
5	C(10)−C(100)	1.466(8)	C(20)−C(102)	1.485(8)
	C(30)−C(200)	1.474(8)	C(40)−C(202)	1.475(8)

	Torsion Angles between the Linked Cp and the Phenyl Mean Planes (deg)	
1o	phenyl C(100) to C(105)	
	Cp ring C(10) to C(14)	68.6(8)
	Cp ring C(20) to C(24)	32.5(8)
3	phenyl C(100) to C(105)	
	Cp ring C(10) to C(14)	12.35(5)
	Cp ring C(20) to C(24)	14.74(5)
5	phenyl C(100) to C(105)	
	Cp ring C(10) to C(14)	14.55(5)
	Cp ring C(20) to C(24)	9.99(5)
	phenyl C(200) to C(205)	
	Cp ring C(30) to C(34)	25.71(5)
	Cp ring C(40) to C(44)	6.84(5)

3. Electrochemical Results. Except for the *o*- and *p*-diferrocenylbenzene, for which the beginning of a splitting is observed, a single oxidation wave appears whatever the technique used. Coulometric measurements indicate that this wave is bielectronic, thus confirming again the compounds' formulas.

Since for each compound the mixed-valence species is in equilibrium with the homovalent ones (eq 1), in order to get the mixed-valent complex absorption spectrum, we first determine the comproportionation constant K_c, adapting a literature procedure.[26]

$$\mathrm{Fc{-}Fc} + \mathrm{Fc^+{-}Fc^+} \rightleftharpoons 2\mathrm{Fc{-}Fc^+}$$

$$K_c = \frac{[\mathrm{Fc{-}Fc^+}]^2}{[\mathrm{Fc{-}Fc}][\mathrm{Fc^+{-}Fc^+}]} \qquad (1)$$

Profiles of the differential-pulse voltammograms are simulated with a home-made program to get the two redox potentials, i.e., $E°_1$ ($\mathrm{Fc{-}Fc^+/Fc{-}Fc}$) and $E°_2$ ($\mathrm{Fc^+{-}Fc^+/Fc{-}Fc^+}$) of the two closely spaced processes. Then K_c can be computed following eq 2, where $\Delta E° = E°_2 - E°_1$ and F is the Faraday constant.

(26) Richardson, D. E.; Taube, H. *Inorg. Chem.* **1981**, *20*, 1278−1285.

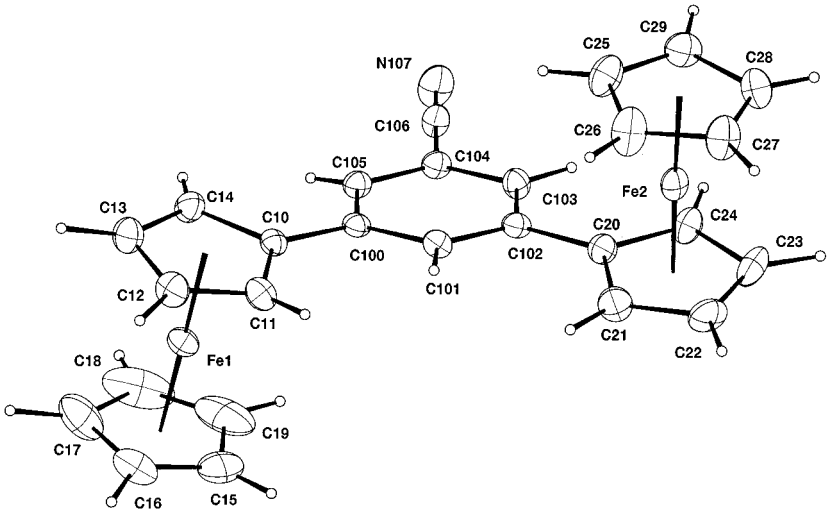

Figure 3. Molecular structure of **5**.

$$K_c = \exp\left(\frac{\Delta E^\circ F}{RT}\right) \qquad (2)$$

Results for the diferrocenylbenzene isomers are summarized in Table 3. For solubility reasons, the *p*-diferrocenylbenzene (**1p**) redox potentials have been determined in $CHCl_3$ instead of CH_3CN.

It is known that K_c values depend on several energetic factors. Among them, the electrostatic interaction between the redox centers, strongly related to their distance, was believed to make the major contribution.[27] As expected, the ortho isomer **1o** shows a higher K_c value than the para one. However, the meta isomer **1m**, in which the Fe−Fe distance is intermediate, gives rise to the smallest K_c value. This indicates that the electrostatic interpretation is not sufficient to explain K_c variations.

For the different substituted *m*-diferrocenylbenzenes, electrochemical results are also displayed in Table 3. In Figure 4 have been plotted their E°_1 and E°_2 values against the Hammett parameters σ_m.[28] As expected, the more electron-withdrawing the substituent is, the more anodic the potentials of the two couples are. Note that the σ_m parameters used here are primary constants describing both inductive and resonance effects. This kind of dependence was in fact already reported many years ago by Hoh *et al.*[29] and Little *et al.*[13a]

For all cases, the ΔE° values remain small; thus all the K_c values fall in the same range, from 21.7 (CN) to 47.8 (NH_2). With this topology, a substituent dependence, albeit weak, is observed, thus showing that an "electronic" influence of the redox centers' bridging unit on the comproportionation constant cannot be ruled out.[8]

4. Intervalence Bands and Experimental V_{ab} Couplings. Determination of the experimental coupling parameter V_{ab} has been achieved by spectroelectrochemistry using a previously described procedure.[3] A stepwise coulometric titration was performed on a *ca.* 2×10^{-3} mol·L^{-1} solution, and UV−vis−near IR absorption spectra were regularly recorded by transferring part of the electrochemical cell content into a UV cuvette for different values of *n* (*n* being the average number of electrons removed, $0 < n < 2$).

However, upon passing the half-oxidation point, a quick decomposition process was observed, the most striking features of which were precipitation of a brown solid and a dramatic color change from deep-green to brown. Such a phenomenon, which occurs in various solvents, such as CH_2Cl_2, DMF, CH_3CN, has been scarcely described in the literature. The role of O_2 has been suspected,[30] as well as the ferrocenium reactivity toward nucleophilic species (i.e., halide ions), and its stability in various solvents.[31] To circumvent this difficulty, we designed a new type of air-tight electrochemical cell, allowing cell content transfers to be realized under *anaerobic conditions*, although one performs an electrochemical oxidation. With this apparatus, and using CH_3CN as solvent, decomposition is only slowed down, and quick electrolyses with a minimal number of stops have to be performed. Typically, from a 50-mL stock solution, six 8-mL fractions were used consecutively. Each fraction was electrolyzed, and only three spectra were recorded: the initial one, an intermediate one for a given *n*, $0 < n < 2$, and the final one for complete oxidation. The experiment was then renewed with a fresh fraction for a new value of n. Around half-oxidation, only the spectrum which displays the most intense intervalence band was used. This procedure yielded correct spectrophotometric measurements even for the fully oxidized stage.

Then, the pure valence-mixed complex spectrum was extracted from the experimental one, by subtracting the homovalent species spectra weighted by their respective proportions using

Table 3. Redox Potentials[a] and K_c Values[b] for Diferrocenylbenzenes and Their Substituted Derivatives

compd	E°_1 (mV)	E°_2 (mV)	K_c
1o	387	518	160
1p	386[c]	490[c]	60[c]
1m	398	488	35
2	379	478	50
3	433	526	35
4	386	470	25
5	459	538	20
6	471	558	30
7	466	551	30

[a] By differential pulse voltammetry with curve fitting, in CH_3CN containing 0.1 M NBu_4PF_6, unless otherwise noted. Values with respect to SCE. [b] From eq 2. [c] In $CHCl_3$.

(27) Sutton, J. E.; Taube, H. *Inorg. Chem.* **1981**, *20*, 3125−3134.
(28) Maskill, H. *The Physical Basis of Organic Chemistry;* Oxford University Press: Oxford, 1985; pp 202−203 and 442−443.
(29) Hoh, G. L. K.; McEwen, W. E.; Kleinberg, J. *J. Am. Chem. Soc.* **1961**, *83*, 3949−3953.
(30) Oxygen-induced ferrocenium decomposition has been reported but with no mechanism proposition. See: Yang, E. S.; Chan, M. S.; Wahl, A. C. *J. Phys. Chem.* **1975**, *79*, 2049−2052.
(31) Prins R.; Korswagen, A. R.; Kortebeek A. G. T. G. *J. Organomet. Chem.* **1972**, *39*, 335−344.

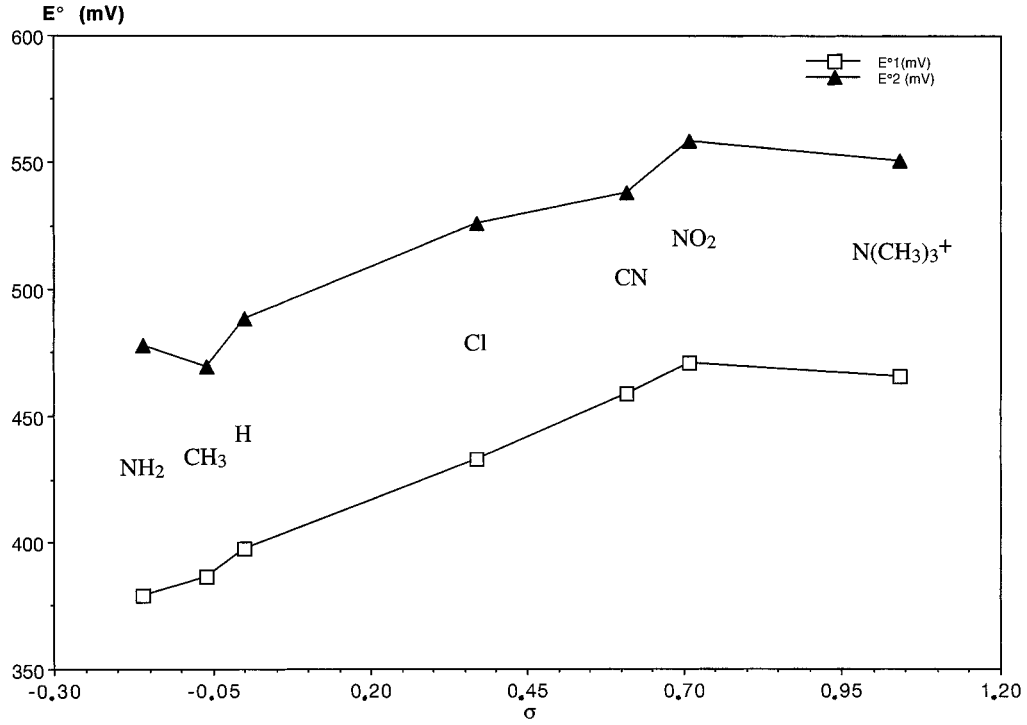

Figure 4. $E°_1$ and $E°_2$ against Hammett parameter.

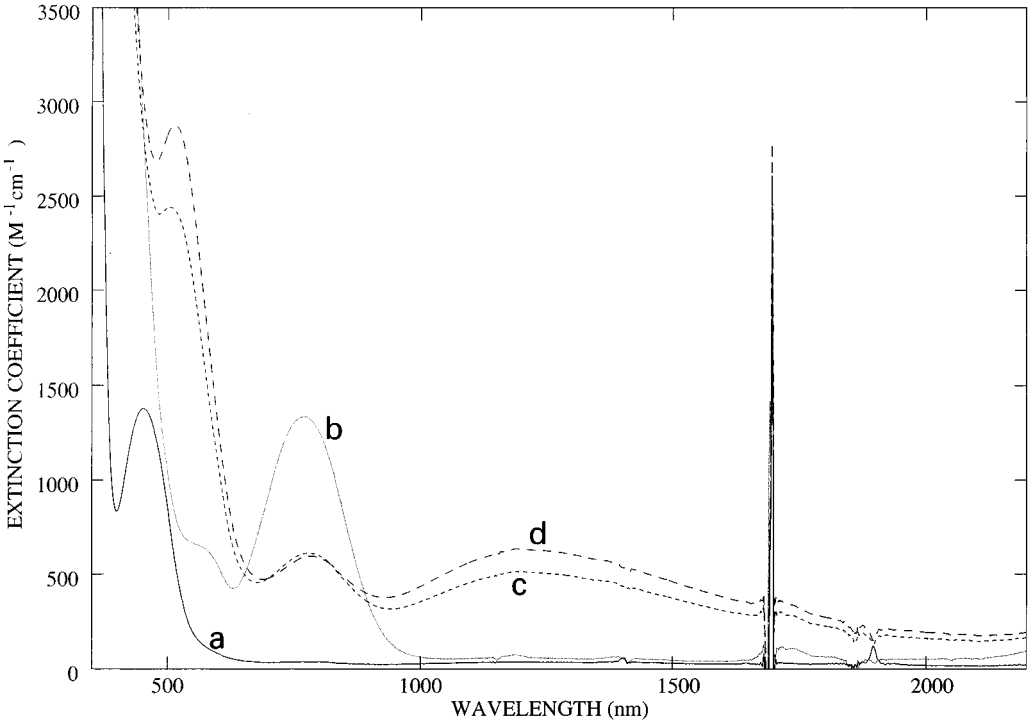

Figure 5. Spectra of the different forms of **1p** recorded in $CHCl_3$: (a) starting form Fc−Fc; (b) fully oxidized form Fc^+−Fc^+; (c) half-oxidized solution (mixture of homovalent and mixed-valence forms); (d) pure mixed-valence form Fc−Fc^+.

the previously determined K_c value. An example of such a treatment is given in Figure 5. Deconvolution of the intervalence band (partly overlapped by a ferrocenium absorption) is performed using an already described home-made program.[3] This gives ϵ_{max}, ν_{max} and $BW_{1/2}$, (respectively molar extinction coefficient, wavenumber at the maximal absorbance, and half-height band width). Finally, the through-space intermetallic distance R_{MM} is determined either from crystallographic data or by molecular modeling using PC-Model,[32] both being in good agreement. With all these parameters, gathered in Table 4, we calculate the V_{ab} coupling constant, using eq 3.[5]

$$V_{ab} = \frac{2.05 \times 10^{-2}}{R_{MM}} \sqrt{\epsilon_{max} BW_{1/2} \bar{\nu}_{max}} \qquad (3)$$

Note that, in eq 3, the definition of the R_{MM} distance can raise some difficulty, and R_{MM} should probably be replaced by the difference in electron centroids in the ground and excited

(32) PCMODEL Serena Sofware, Box 3076, Bloomington, IN 47402-3076.

Table 4. Spectroscopic Results[a] (Position,[b] Extinction Coefficient,[b] and Width[b] of the Intervalence Transitions) and Experimental[c] and Theoretical[d] V_{ab} Couplings

				V_{ab} (eV)	
compd	$\bar{\nu}_{max}$ (cm^{-1})	ϵ_{max} ($M^{-1}\cdot cm^{-1}$)	$BW_{1/2}$ (cm^{-1})	exptl	calcd
1o	6540 ± 620	91 ± 5	6750 ± 230	0.025 ± 0.002	
1p	7450 ± 180[e]	620 ± 20[e]	4906 ± 16[e]	0.043 ± 0.001	0.0768
1m	8290 ± 100	46 ± 5	4040 ± 140	0.013 ± 0.001	0.0110
2	5360 ± 600	29 ± 3	7725 ± 45	0.011 ± 0.001	0.0079
3	8340 ± 100	32 ± 3	4590 ± 150	0.011 ± 0.001	0.0107
4	8170 ± 120	56 ± 5	4440 ± 50	0.015 ± 0.001	0.0108
5	8710 ± 580	28 ± 3	5220 ± 500	0.012 ± 0.002	0.0117
6	8380 ± 180	35 ± 7	5780 ± 360	0.013 ± 0.002	0.0122
7	9000 ± 600	32 ± 5	4770 ± 500	0.012 ± 0.002	0.0113

[a] In CH_3CN containing 0.1 M NBu_4PF_6 unlesss otherwise noted. [b] From spectral simulation. [c] From eq 3. [d] Calculated for planar conformations only. [e] In $CHCl_3$.

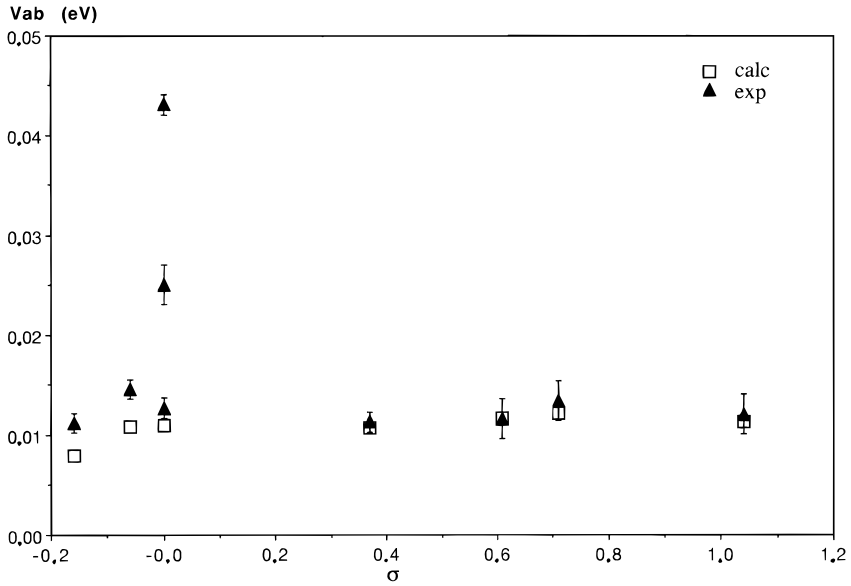

Figure 6. V_{ab} couplings against Hammett parameter: experimental and theoretical values (from extended Hückel calculations).

states.[33] However, in the present case where wave functions are strongly localized on metal d orbitals, and since we are mainly interested by comparisons, this distinction does not matter.

V_{ab} couplings are shown in Figure 6 as functions of the σ Hammett parameter arranging substituent groups from strong donors to strong acceptors. There is clearly a great influence of the nature of the isomer of diferrocenylbenzene on the coupling value, the lowest value being obtained for the meta disposition. For the substituted compounds of the **1m** family, no systematic variation can be experimentally detected, taking into account the uncertainty of the measurements.

5. V_{ab} Couplings: a Rationalization. Electronic coupling is the key parameter describing the efficiency of the molecule to perform intramolecular electron transfer. It was measured here indirectly by the intervalence transition, but corresponds to a process occurring normally at the crossing point of Hush−Marcus curves.[1] At this crossing point, we have demonstrated elsewhere that V_{ab} is given by the fundamental frequency ν_{ab} of the back and forth oscillation process of the charge through the ligand between the two metal sites.[34] This oscillation occurs in competition with the trapping of the charge on one of these two sites by the progressive distortion of their coordination sphere and environment. At this crossing point $V_{ab} = h\,\nu_{ab}/2$. Note that V_{ab} can also be obtained from the avoided crossing between adiabatic potential energy curves (the energy splitting), because diagonalizing the Hamiltonian at the crossing point between the diabatic curves is equivalent by the effective Hamiltonian Technique to extracting ν_{ab}.[34,35] Before analyzing in detail the time evolution of an electron transfer process in a multibranched ligand to interpret the V_{ab} variation observed experimentally, we need to identify the specific energy levels (channels) of the ligand participating in the transfer for our particular class of compounds.

5.1. Molecular Orbitals Controlling the Couplings. The diferrocenyl compounds can be formally decomposed into a free ligand of the bis(cyclopentadiene) type and two iron atoms. Metal orbitals of the $d_{x^2-y^2}$ type can overlap with C(2p) orbitals of π symmetry of the bridgehead carbon atoms of the cyclopentadienyl rings (see Figure 7).[36] Then the interaction of the filled and empty orbitals of the ligand with iron orbitals raises the degeneracy between symmetry-adapted linear combinations of the metal orbitals. In the final diagram, there is an electron hole in the pair of $d_{x^2-y^2}$ orbitals for the mixed-valence compound.[36] Thus V_{ab} is determined from the energy splitting

(33) Oh, D. H.; Sano, M.; Boxer, S. G. *J. Am. Chem. Soc.* **1991**, *113*, 6880−6890. Reimers, J. R.; Hush, N. S. In *Mixed Valency Systems: Applications in Chemistry, Physics and Biology*; Prassides, K., Ed.; Kluwer Acad. Publ.: Dordrecht, 1991; pp 29−50. Cave, R. J.; Newton, M. D. *Chem. Phys. Lett.* **1996**, *249*, 15−19. Karki, L.; Lu, H. P.; Hupp, J. T. *J. Phys. Chem.* **1996**, *100*, 15637−15639.

(34) Joachim, C.; Launay, J.-P.; Woitellier, S. *Chem. Phys.* **1990**, *147*, 131−141.

(35) Woitellier, S.; Launay, J.-P.; Joachim, C. *Chem. Phys.* **1989**, *131*, 481−488.

(36) Boukheddaden, K.; Linares, J.; Bousseksou, A.; Nasser, J.; Rabah, H.; Varret, F. *Chem. Phys.* **1993**, *170*, 47−55.

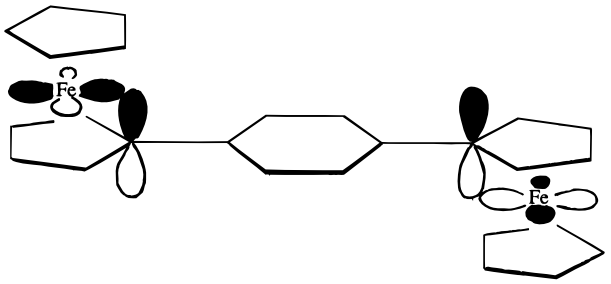

Figure 7. Overlap of $d_{x^2-y^2}$ type metal orbitals (z taken as the main axis of the ferrocene group) with C $2p_z$ bridgehead orbitals in the case of **1p**.

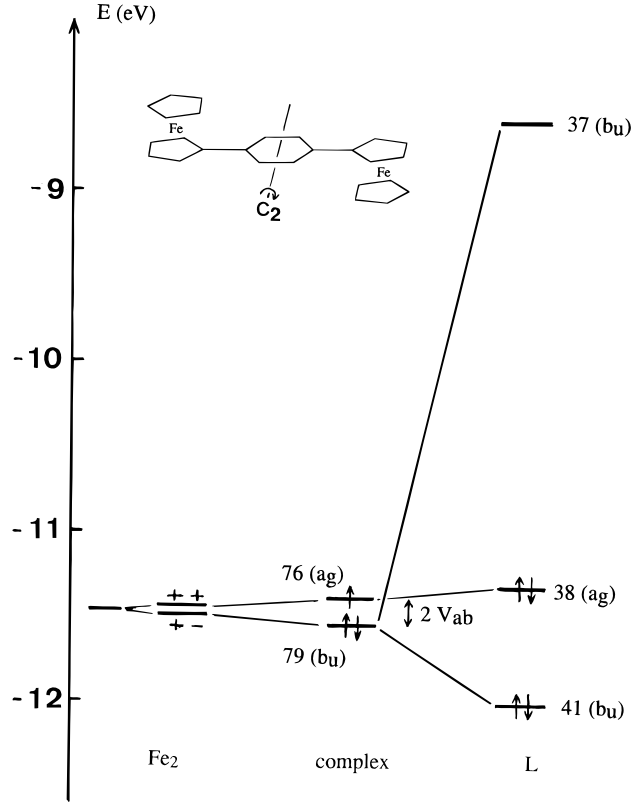

Figure 8. Interaction diagram for **1p.** + + and + − designate the symmetry adapted linear combinations of iron $d_{x^2-y^2}$ orbitals. L is the bis(cyclopentadienyl)benzene ligand.

(see Figures 8 and 9). In the following, only the case of para and meta isomers will be discussed, because in their structures the conjugated systems are more or less planar, while for the ortho isomer **1o** a severe deviation to planarity occurs, which precludes a simple orbital interpretation.

Para Isomer. For the para isomer **1p** (C_{2h} point group) the interaction diagram is shown in Figure 8. The two metal orbitals able to mix with the ligand are of the $d_{x^2-y^2}$ type. For the Fe_2 fragment, they give the two symmetry-adapted linear combinations (SALCs) $2^{-1/2}(d_{x^2-y^2} + d_{x^2-y^2})$ and $2^{-1/2}(d_{x^2-y^2} - d_{x^2-y^2})$, which are quasi-degenerate, taking into account the weakness of the direct metal−metal overlap. These SALCs will be noted "+ +" and "+ −" in the following and are respectively symmetrical (a_g) and antisymmetrical (b_u) with respect to the C_2 axis of the molecule (see Figure 8). Then each of the SALCs "selects" ligand orbitals of the same symmetry to interact. It should be noted that some ligand orbitals have almost no weight on the bridgehead carbon atoms and, thus, play no role in the interaction.

The + − combination of metal orbitals interacts with the filled orbital 41 and the empty 37 of the free ligand. Thus the

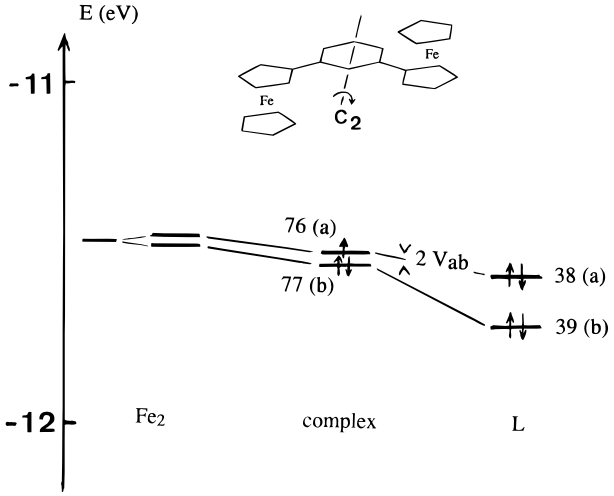

Figure 9. Interaction diagram for **1m**. The vacant ligand orbitals are too high in energy and not represented.

final MO (79) has very small weights on the ligand as a result of cancellation effects. It is slightly stabilized with respect to pure metal orbitals.

The + + combination of metal orbitals interacts mainly with ligand orbital 38 (the interaction with a vacant ligand orbital of the same symmetry, 35, is possible but can be neglected due to a large energy gap). Since orbital 38 is filled, a net destabilization occurs, giving MO 76. The shape of orbital 76 shows indeed an appreciable contribution coming from ligand 38.

Thus the electronic interaction is due to the different perturbations experienced by the + + and + − SALCs of Fe orbitals when they mix with the ligand orbitals.

Meta Isomer. A similar analysis can be performed for the meta isomer (C_2 point group). Here also, all MO can be classified using their symmetry properties with respect to a C_2 axis (see Figure 9). The crucial ligand orbitals are then 38 (a symmetry) and 39 (b symmetry), which present almost the same energies and very similar weights on the bridgehead carbon atoms. Thus they interact in almost the same way with + + and + − SALCs, giving the final MO 76 and 77. Consequently, their energy difference is very small, corresponding to a very small V_{ab}. Here the vacant ligand orbitals are too high to mix efficiently.

Effects of Substitution on the Meta Isomer. While no clear variation of V_{ab} with the substituent can be proved experimentally, theoretical calculations predict a modest increase of the coupling when passing from a donor substituent (NH_2) to an acceptor one (NO_2), as shown in Table 4 and Figure 6. (Curiously, this tendency does not carry on for the strongly accepting $N(CH_3)_3^+$ group.) This small variation could be understood by a detailed examination of MO 76 and 77. Thus in unsubstituted *m*-diferrocenylbenzene, MO 76 is slightly above 77. MO 76 has practically a node on carbon atoms 2 and 5 for symmetry reasons, while 77 has a strong contribution from C(2) and a minor one from C(5) (see Figure 10). Consequently, the introduction of a donor or acceptor substituent in position 5 can change slightly the energy of MO 77, but not of 76. With a donor group such as NH_2, MO 77 is lifted, and thus V_{ab} decreases. Conversely, with an acceptor group like NO_2, MO 77 is stabilized, and the energy gap with 76 increases.

Finally, since one of the MO defining the coupling has a strong contribution from C(2), the effect of substitution on this position should be appreciable, and higher than for a substitution in the 5-position. However, it is not easy to introduce substituents in this position for obvious steric reasons, and in

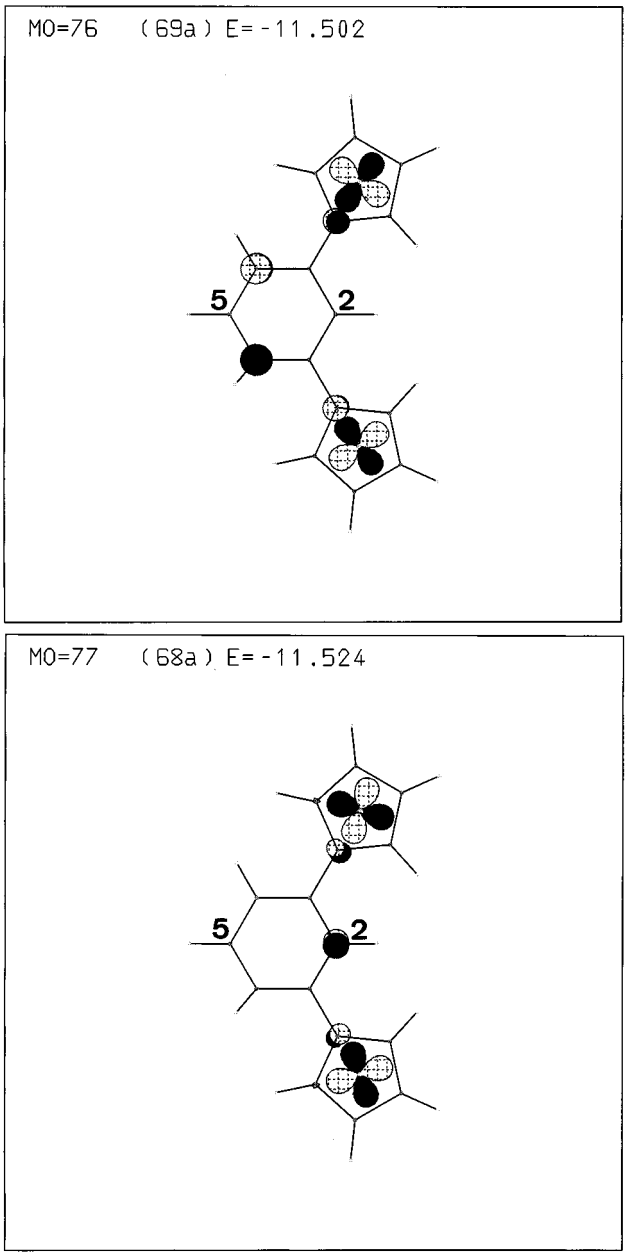

Figure 10. Shape of MO 76 and 77 in **1m**. The contributions of the outer cyclopentadienyl rings are not shown. The contribution of C(5) to MO 77 is too small to be drawn.

addition, they could introduce an additional direct coupling path in the electron transfer process.

5.2. Quantum Interference Interpretation. The weakness of the interaction in the meta isomer is due to a cancellation effect: the interaction with one ligand orbital alone (either 38 or 39) would give a nonzero V_{ab}, but the simultaneous presence of the two coupling paths with different symmetries destroys the overall coupling. This is strongly reminiscent of an interference effect and can be understood by the time dependent analysis of the through-bond charge transfer process. In the following, a detailed comparison will be made between two model systems: a three-state system, for which no quantum interference can occur, and a four-state system, for which quantum interference is possible.

The simplest quantum system to model a through-bond electron transfer process is the three-state system (Figure 11), each level representing the total molecular energy for initial, final, and intermediate states during the transfer process, i.e., for an electron or hole localized either on the ends or on the

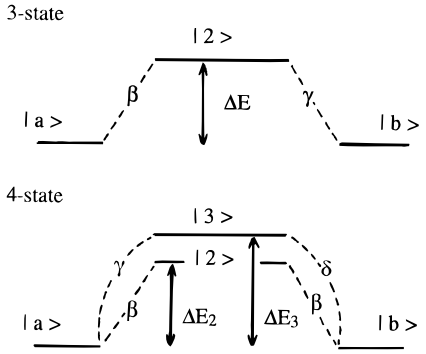

Figure 11. Energetic models of a three-state and a four-state system. β, γ, and δ are the couplings while ΔE, ΔE_2, and ΔE_3 are the differences in energy when the electron (or hole) is localized either on the terminal sites or on the bridge.

bridging part. The basic parameters are then ΔE, the energy difference between the terminal and ligand states, and β and γ, the couplings at each end of the ligand. To make the link with the MO model at the monoelectronic level, β and γ are taken proportional to the coefficients of the ligand MO on the bridgehead carbon atoms, and in particular they are *algebraic quantities*, which introduces the possibility to describe different symmetries of the ligand states.

The four-state system presented in Figure 11 can be used to model substituted molecules of the **1m** family, taking into account the existence of two coupling channels with different symmetries (ligand MO 38 and 39). The two ligand states are taken of almost equal energy, and a phase shift can be generated by choosing $\delta = -\gamma$ on one of the two intermediate states. This will define the phase-modulated branch in which one can in principle play with the energy of this level or the coupling amplitude to control the influence of this dephasor branch.

We now compare the time evolutions when, at $t = 0$, the systems are prepared in state $|a\rangle$. From the time-dependent Schrödinger equation, one computes the $g_b(t)$ probability amplitude to reach state $|b\rangle$[37] (note that $g_b(t)$ is a complex quantity carrying a modulus and a phase). The details of calculation are given in the Appendix. Then $|g_b(t)|^2$ represents the probability at time t for the system to reach state $|b\rangle$, and this quantity is plotted as a function of time in Figure 12, enabling a direct comparison of the two systems. Usually one recognizes an oscillating behavior characterized by a fundamental frequency ν_{ab} governing the secular evolution of the transfer process.[34] V_{ab} is then simply given by $V_{ab} = h\nu_{ab}/2$.

The time evolution of the three-state system is given in Figure 12a. The calculation shows that $g_b(t)$ itself contains a time-independent prefactor $2\,\beta\gamma/(\beta^2 + \gamma^2)$. This prefactor is also interesting to consider even if not experimentally accessible in an intervalence band measurement.[38] When $\gamma = \pm\beta$, which is the case here because we consider symmetrical systems, this time-independent prefactor is maximum giving rise to a resonant transfer process ($|g_b(t)|^2$ can reach unity even if state $|2\rangle$ is not at the same energy as states $|a\rangle$ and $|b\rangle$).[37] But there is a π phase shift between the $\gamma = \beta$ and the $\gamma = -\beta$ cases. This phase shift is not observable (i.e., has no consequences on $|g_b(t)|^2$) in a three-state system since there is only one open electron

(37) Sautet, P.; Joachim, C. *J. Phys. C: Solid State Phys.* **1988**, *21*, 3939−3957. Note that in this paper the probability is denoted $g(t)$, but corresponds actually to $|g_b(t)|^2$ here.

(38) The intervalence band intensity is determined by the frequency of the main component in the time evolution $|g_b(t)|^2$, but does not depend upon the time-independent prefactor. To obtain the latter, it would be necessary to follow in real time the dynamic evolution of the system, by ultrafast laser techniques.

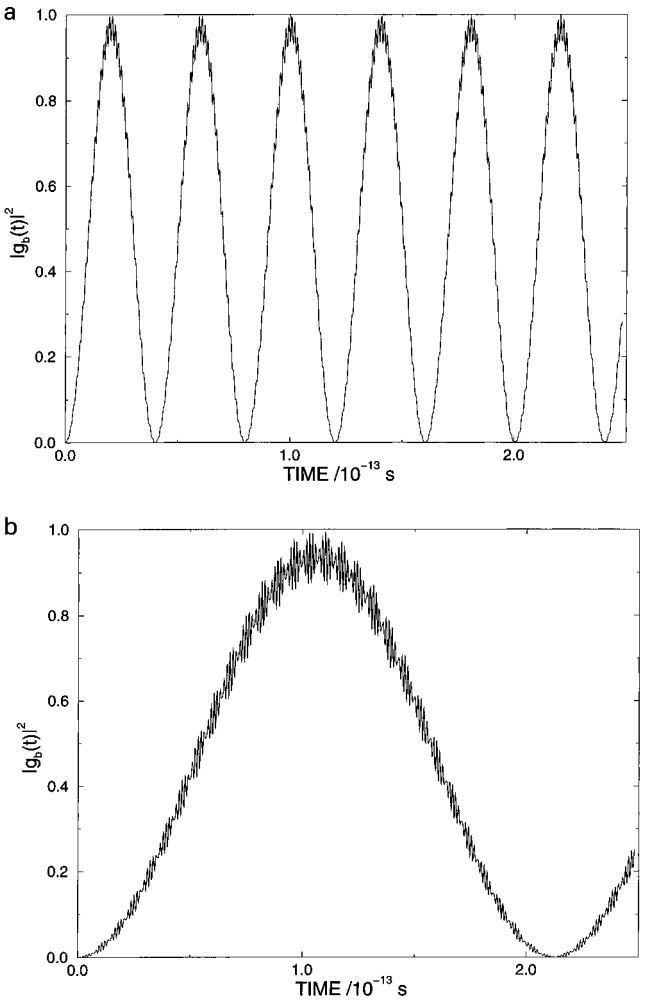

Figure 12. Time evolutions $|g_b(t)|^2$ for the three-state (a) and four-state (b) systems. Parameters for a: $\beta = 0.4$ eV; $\Delta E = 3.0$ eV corresponding to $V_{ab} = 0.05$ eV. For b: $\beta = \gamma = 0.4$ eV; $\delta = -0.4$ eV; $\Delta E_2 = 2.7$ eV; $\Delta E_3 = 3.3$ eV.

transfer channel via state $|2\rangle$. However, for more than one open channel, this phase shift has observable consequences as shown below.

The four-state system evolution is shown in Figure 12b. It can been obtained either from numerical calculation or from an analytical solution,[39] depending on the input parameters (see Appendix). When the conditions $\gamma = \beta$, $\delta = -\gamma$, and $\Delta E_2 = \Delta E_3$ are approached, the time-independent prefactor of $|g_b(t)|^2$ does not go to 0. But the fundamental frequency of the process goes to 0, that is, V_{ab} is very small (see Figure 12b: *compared with the three-state system and for similar parameters, the period is much longer*). At the same time all the independent amplitudes of the sinusoids combine in such a way that their sum goes to 0 before ν_{ab} equals 0 (note that this does not happen for $\delta = \gamma$). This is clear evidence that the dephasing branch acts at the same time on the mixing and on the frequency of the elementary time processes involved in the transfer. Experimentally, this is the sharp decrease of ν_{ab} (and thus of V_{ab}) with a small δ variation which is characteristic of an interference effect, one branch being the dephasor. This is fortunate because, without this quantum phenomenon of changing all the quantum states of a system by only modifying one of its elementary parameters, the only possibility to prove an interference effect would have been to follow experimentally the time evolution of the system during the transfer process, which is much more demanding than just measuring V_{ab}.

To summarize, the consequence of an interference effect in a ligand is the variation of V_{ab} depending on the coupling sign and energy in one branch compared to the others. Thus the ΔE_2 and ΔE_3 parameters are related to the energy of the ligand orbitals such as 38 and 39. Although the frequency of the oscillation process ν_{ab} changes when the two coupling paths are simultaneously present, one recognizes the basic behavior of an interferometer. The main difference with a macroscopic interferometer is that adding one branch to a quantum system not only introduces a possibility of interference but also modifies all its quantum states, i.e., its characteristic frequencies. This means that the superposition operation, which is the basis of conventional interference, is more difficult to trace, the frequency of the oscillation process through the intermediate states being also changed. The important result is nevertheless the following: since the oscillation frequency ν_{ab} determines V_{ab}, which itself determines the intensity of the intervalence transition, there is indeed, under certain conditions fulfilled by the ligand orbitals, an extinction of an experimental signal when the two branches contribute to electron transfer.

Conclusion

The series of the three isomers **1o**, **1m**, and **1p** of diferrocenylbenzene shows a strong influence of the molecular topology on the electronic V_{ab} coupling. This is particularly evident when comparing **1m** and **1p** which exhibit planar geometries, and for which electron transfer can occur only via through-bond coupling. This difference in coupling is rationalized by molecular orbital calculations at the extended Hückel level. For compounds of the **1m** family, the effect of substitution in the 5-position is not detected experimentally, although extended Hückel calculations predict a very small effect.

The weakness of the interaction in **1m** can be ultimately traced to a quantum interference effect, i.e., a cancellation of the contributions of two electron transfer paths, each one corresponding to a coupling with a given ligand orbital. This concept seems at first sight surprising because the frequency of charge oscillation is modified when the two paths are present. But at the same time, the probability $|g_b(t)|^2$ of the charge transfer process changes, too, which is the true signature of an interference.

Although the influence of substitution is minor in the present case, this thorough analysis of the coupling mechanism could help in the design of more efficient systems to control intramolecular electron transfer.

Experimental Section

Materials. All solvents and chemicals for synthesis were commercially available of reagent grade quality and were used without any further purification except as noted below. Tetrahydrofuran (THF) and diethyl ether were freshly distilled from sodium benzophenone. Dimethoxyethane (DME) was passed over neutral alumina prior to use. Petroleum ether refers to the fraction boiling from 35 to 50 °C. Solvents were removed on a rotary evaporator at water-aspirator vacuum, and remaining traces were then removed on a vacuum pump. Experiments involving air- or water-sensitive reagents were carried out using standard Schlenk tube techniques under an argon atmosphere. For electrochemistry, acetonitrile was from Merck (Uvasol), while $CHCl_3$ was passed on alumina.

Methods and Instrumentation. UV−vis−Near IR spectra were taken on a Shimadzu UV-3100 spectrophotometer. ^{1}H NMR spectra were recorded on a Bruker WF-250 spectrometer and processed with the program SwaN-MR.[40] Chemical shifts were measured with reference to the residual solvent signals. Mass spectra (EI and FAB, NBA matrix) were recorded on a Nermag R10-R10 spectrometer.

(39) Joachim, C. Unpublished calculations.

(40) Balacco, G. *J. Chem. Inf. Comput. Sci.* **1994**, *34*, 1235−1241.

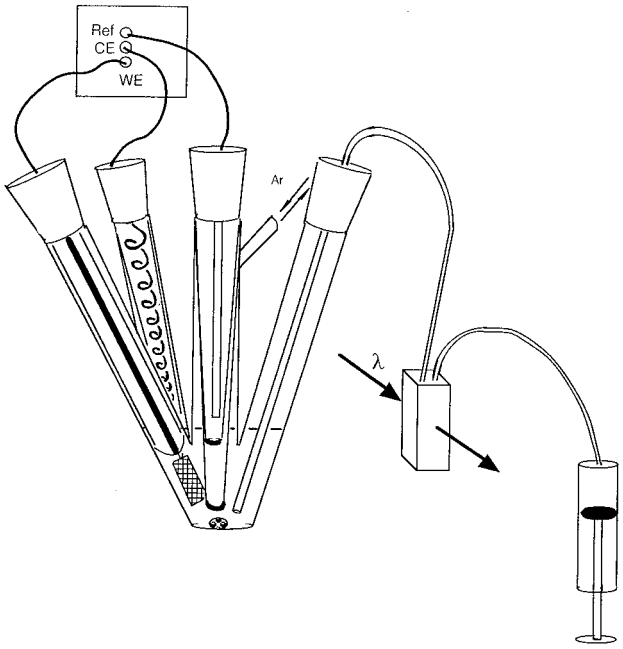

Figure 13. Electrochemical cell used for spectroelectrochemistry.

Electrochemical measurements were performed with an Electromat 2000 system (ISMP technology). For all electrochemical techniques, the reference electrode was a saturated potassium chloride calomel reference electrode (Tacussel) separated from the nonaqueous solution by an intermediate compartment. Water and Cl^- contamination were negligible for the time scale of the experiments. Cyclic voltammograms was obtained using a platinum disk (1 mm diameter) as the working electrode and a platinum wire as the auxiliary electrode. Linear and differential-pulse voltammetry were carried out using a rotating platinum electrode (Metrohm) at 1000 rpm. The pulse parameters were as follows: amplitude, 48 mV; duration, 50 ms; interval between pulses, 0.2 s. Differential pulse voltammograms were simulated with a homemade program taking into account the pulse amplitude, to get $\Delta E°$ and K_c.

Coulometric investigations were performed under argon in a three-electrode four-neck cell improved in the laboratory (Figure 13): the reference electrode and the counter electrode (a platinum spiral) were separately immersed in the solvent (CH_3CN) containing the supporting electrolyte (0.1 M tetrabutylammonium hexafluorophosphate recrystallized twice from ethanol) and isolated from the bulk solution by a glass frit. The working electrode was a platinum grid (*ca.* 2 cm^2 area). Coulometry was typically performed on an 8-mL scale. In the last side arm of the cell was inserted a Teflon tubing, dipping in the solution, and connected to a degassed 10-mL syringe via the spectrophotometric flow-cell located in the spectrophotometer. Transfers of the solution to the spectrophotometer were obtained by pumping the electrochemical cell content into the UV cuvette with the syringe. Once the spectrum was recorded, the UV cell content was returned to the electrochemical cell by pushing backward the syringe plunger.

1,4-Diferrocenylbenzene (1p). Monobromoferrocene[16] (773 mg, 2.92 mmol) was converted into ferrocenyllithium in ether (50 mL) at −78 °C with ^{t}BuLi (1.7 M in pentane, 4.12 mL, 7 mmol), and the solution was allowed to warm to room temperature for 40 min. Ether was then removed on the vacuum line and replaced by THF (12 mL) followed by the addition of a solution of $ZnCl_2$ (400 mg, 2.92 mmol) in THF (3 mL). The resulting solution was stirred at room temperature for 30 min. In a three-neck round-bottom flask, equipped with a magnetic stirring bar and a condenser, 1,4-diiodobenzene (463 mg, 1.4 mmol) and tetrakis(triphenylphosphine)palladium (77 mg, 0.067 mmol) were dissolved in THF (10 mL). The ferrocenylzinc chloride solution (2.92 mmol) was then transferred via a cannula into the diiodobenzene solution. The mixture was stirred at room temperature for 17 h and heated under reflux for 1 h. The reaction was quenched with 70 mL of 10% HCl, and the solid, which is very poorly soluble, was extracted with 150 mL of $CHCl_3$, washed with H_2O, and recrystallized from $CHCl_3$. Yield: 57%. ^{1}H NMR ($CDCl_3$): δ 4.09 (10 H, s), 4.36 (4 H, s), 4.69 (4 H, s), 7.33 (4 H, s). Mass spectrum (EI): m/z = 446 (100, M). Anal. Calcd for $C_{26}H_{22}Fe_2$: C, 69.98; H, 4.98. Found: C, 69.34; H, 4.88.

2-Ferrocenyl-1,3,2-dioxaborolane (9). To an ice-cooled (0 °C) solution of ferrocene (8 g, 43 mmol) in THF (40 mL) in a Schlenk tube was added ^{t}BuLi (1.7 M in pentane, 25.3 mL, 43 mmol) slowly via a syringe. The resulting suspension was stirred at this temperature for 10 min and then allowed to warm to room temperature for 30 min. The mixture was cooled to −78 °C, and $B(OBu)_3$ (13.9 mL, 51.6 mmol) was slowly added via a syringe. After 10 min at −78 °C, the solution was stirred for 2 h at room temperature and hydrolyzed with 10 mL of 5% HCl at 0 °C. Ether was added, and the mixture was filtered through a Celite pad. The organic layer was separated from the filtrate, washed with brine, and dried over magnesium sulfate and solvents were evaporated. Chromatography on neutral alumina gave ferrocene (with toluene as eluent) and ferrocenylboronic acid (toluene/MeOH, 95/5). The latter was dissolved in toluene (100 mL) with ethylene glycol (2.4 mL, 43 mmol), and the solution was heated under reflux for 2 h. The solution was filtered on paper, the solvent was evaporated, and the solid was dried under vacuum to give an orange, fluffy and stable solid. Yield: 53%. ^{1}H NMR ($CDCl_3$): δ 4.14 (5 H, s), 4.32 (4 H, s), 4.41 (2 H, t, J = 1.5 Hz), 4.42 (2 H, t, J = 1.5 Hz). Mass spectrum (EI): m/z = 256 (100, M). Anal. Calcd for $C_{12}H_{13}BFeO_2$: C, 56.25; H, 5.08. Found: C, 56.67; H, 4.94.

3,5-Dibromobenzonitrile (11). 4-Aminobenzonitrile (3 g, 25.39 mmol) was dissolved in glacial acetic acid (15 mL) in a 500-mL Erlenmeyer, and the solution was ice-cooled. Bromine (2.62 mL, 50.79 mmol) was added to the suspension and the mixture allowed to warm to room temperature. Precipitation of the crude 4-amino-3,5-benzonitrile (**10**) was obtained upon addition of H_2O (300 mL). After being removed by filtration, washed with water, and air-dried, it was used without any further purification for deamination.

In a 100-mL round-bottom flask, 4-amino-3,5-dibromobenzonitrile (*ca*. 25.39 mmol) was dissolved in hot EtOH (20 mL), and 95% H_2SO_4 (2.61 mL, 50.78 mmol) was added to the boiling solution. After removal of the oil bath, powdered sodium nitrite (2.63 g, 38.08 mmol) was added. The solution was stirred for 15 min and heated under reflux until gas evolution stopped. The suspension was then cooled to 0 °C, and the solid was filtered off and rinsed with a minimum amount of EtOH and then H_2O. Purification of 3,5-dibromobenzonitrile (**11**) was achieved by column chromatography on silica gel eluting with petroleum ether/CH_2Cl_2 (50/50) followed by recrystallization from EtOH. Yield: 94%. ^{1}H NMR ($CDCl_3$): δ 7.73 (2 H, d, J = 1.75 Hz), 7.91 (1 H, t, J = 1.7 Hz). Mp: 100 °C (lit.[41] mp 96.5 °C).

3,5-Dibromochlorobenzene (12). The same procedure allowed us to obtain 3,5-dibromochlorobenzene from 2,6-dibromo-4-chloroaniline. The crude product was purified by column chromatography on silica gel eluting with petroleum ether/CH_2Cl_2 (97/3). Yield: 68%. ^{1}H NMR (DMSO-d_6): δ 7.91 (2 H, d, J = 1.65 Hz), 7.98 (1 H, t, J = 1.7 Hz). Mp: 98 °C (lit.[42] mp 99.5 °C).

3,5-Dibromonitrobenzene (13). The same procedure allowed us to obtain 3,5-dibromonitrobenzene from 2,6-dibromo-4-nitroaniline. The crude product was purified by column chromatography on silica gel eluting with petroleum ether and recrystallized from EtOH. Yield: 71 %. ^{1}H NMR (DMSO-d_6): δ 8.50 (1 H, t, J = 1.65 Hz), 8.52 (2 H, d, J = 1.6 Hz). Mp: 104 °C (lit.[43] mp 104.5 °C). Mass spectrum (EI): m/z = 281 (100, M). Anal. Calcd for $C_6H_3Br_2NO_2$: C, 25.64; H, 1.07; N, 4.99. Found: C, 25.67; H, 1.16; N, 4.77.

Standard Procedure for the Cross Coupling under Aqueous Conditions. Dihalobenzene (4 mmol), 2-ferrocenyl-1,3,2-dioxaborolane (2.05 g, 8 mmol), and the catalyst (bis(diphenylphosphino)-ferrocene)palladium(II) chloride (65 mg, 0.08 mmol) were placed in a Schlenk tube equipped with a magnetic stirring bar. Then, DME (30 mL) and aqueous sodium hydroxide (16 mL of 3 M) degassed with argon were added. The Schlenk was tightly closed with a greased glass cap and the solution heated to reflux for 48 h. After cooling, H_2O (50 mL) and $CHCl_3$ (200 mL) were added to the mixture. The organic layer was separated, washed with H_2O, and dried over magnesium

(41) Bogert, M. T.; Hand, W. F. *J. Am. Chem. Soc*. **1903**, *25*, 935−947.
(42) Hurtley, W. H. *J. Chem. Soc.* **1901**, *79*, 1293−1305.
(43) Koerner, W. *Gazz. Chim. Ital.* **1874**, *4*, 305−446.

sulfate. Solvents were removed, and the crude product was purified by column chromatogaphy on silica gel, eluting with petroleum ether/dichloromethane (90/10), and recrystallized from hexane/dichloromethane.

1,3-Diferrocenylbenzene (1m): from 1,3-dibromobenzene. Yield: 58%. ^{1}H NMR ($CDCl_3$): δ 4.06 (10 H, s), 4.33 (4 H, t, $J = 1.66$ Hz), 4.67 (4 H, t, $J = 1.7$ Hz), 7.2 (1 H, dd, $J_{d1} = 6.34$ Hz, $J_{d2} = 8.71$ Hz), 7.29 (1 H, d, $J = 1.44$ Hz), 7.39 (1 H, t, $J = 1.69$ Hz), 7.57 (1 H, t, $J = 1.6$ Hz). Mass spectrum (EI): $m/z = 446$ (100, M). Anal. Calcd for $C_{26}H_{22}Fe_2$: C, 69.98; H, 4.98. Found: C, 69,83; H, 5.06.

1,2-Diferrocenylbenzene (1o): from 1,2-diiodobenzene. Yield: 8%. ^{1}H NMR (DMSO-d_6): δ 4.15 (10 H, s), 4.18 (4 H, t, $J = 1.83$ Hz), 4.28 (4 H, t, $J = 1.84$ Hz), 7.35 (2 H, dd, $J_{d1} = 5.80$ Hz, $J_{d2} = 3.39$ Hz), 7.87 (2 H, dd, $J_{d1} = 5.85$ Hz, $J_{d2} = 3.38$ Hz). Mass spectrum (EI): $m/z = 446$ (100, M). Anal. Calcd for $C_{26}H_{22}Fe_2$: C, 69.98; H, 4.98. Found: C, 69.99; H, 4.71.

3,5-Diferrocenylchlorobenzene (3): from 3,5-dibromochlorobenzene (**12**). Yield: 64%. ^{1}H NMR (DMSO-d_6) δ 4.05 (10 H, s), 4.40 (4 H, t, $J = 1.83$ Hz), 4.96 (4 H, t, $J = 1.83$ Hz), 7.37 (2 H, d, $J = 1.46$ Hz), 7.62 (1 H, t, $J = 1.47$ Hz). Mass spectrum (EI): $m/z = 480$ (100, M). Anal. Calcd for $C_{26}H_{21}ClFe_2$: C, 64.94; H, 4.37. Found: C, 64.81; H, 4.07.

3,5-Diferrocenylnitrobenzene (6): from 3,5-dibromonitrobenzene (**13**). Yield: 64%. ^{1}H NMR ($CDCl_3$): δ 4.08 (10 H, s), 4.42 (4 H, t, $J = 1.90$ Hz), 4.74 (4 H, t, $J = 1.90$ Hz), 7.80 (1 H, t, $J = 1.56$ Hz), 8.08 (2 H, d, $J = 1.63$ Hz). Mass spectrum (EI): $m/z = 491$ (100, M). Anal. Calcd for $C_{26}H_{21}Fe_2NO_2$: C, 63.58; H, 4.28; N, 2.85. Found: C, 63.98; H, 4.36, N, 2.82.

3,5-Diferrocenyltoluene (4): From 3,5-dibromotoluene. Yield: 52%. ^{1}H NMR ($CDCl_3$): δ 2.37 (3 H, s) 4.08 (10 H, s), 4.33 (4 H, s), 4.67 (4 H, s), 7.08 (2 H, s), 7.38 (1 H, s). Mass spectrum (EI) $m/z = 460$ (100, M). Anal. Calcd for $C_{27}H_{24}Fe_2$: C, 70.43; H, 5.22. Found: C, 70.23; H, 5.05.

3,5-Diferrocenylbenzonitrile (5). A stirred suspension of 3,5-dibromobenzonitrile **11** (750 mg, 2.87 mmol), 2-ferrocenyl-1,3,2-dioxaborolane (**9**) (1.47 g, 5.75 mmol), anhydrous powdered potassium phosphate (1.675 g, 7.9 mmol), and (bis(diphenylphosphino)ferrocene)-palladium(II) chloride (42 mg, 0.058 mmol) in argon-degassed DME (28 mL) in a tightly closed (greased glass cap) Schlenk tube was heated to reflux for 48 h. After cooling, saturated aqueous potassium chloride (50 mL) and $CHCl_3$ (250 mL) were added to the mixture. The organic layer was separated, washed twice with saturated aqueous potassium chloride, and dried over magnesium sulfate. Solvents were removed, and the crude product was purified by column chromatogaphy on silica gel, eluting with petroleum ether/dichloromethane (60/40), and recrystallized in hexane/dichloromethane. Yield: 52%. ^{1}H NMR ($CDCl_3$): δ 4.07 (10 H, s), 4.40 (4 H, t, $J = 1.90$ Hz), 4.67 (4 H, t, $J = 1.90$ Hz), 7.53 (2 H, d, $J = 1.65$ Hz), 7.71 (1 H, t, $J = 1.72$ Hz). Mass spectrum (EI): $m/z = 471$ (100, M). Anal. Calcd for $C_{27}H_{21}Fe_2N$: C, 68.79; H, 4.46; N, 2.97. Found: C, 69.41; H, 4.26; N, 2.93.

3,5-Diferrocenylaniline (2). In a 30-mL glass test tube equipped with a magnetic stirring bar, 3,5-diferrocenylnitrobenzene (**6**) (100 mg, 0.204 mmol) was dissolved in hot EtOH (6 mL) and 10% Pd/C (4 mg) was added to the solution. Then a solution of 55% aqueous N_2H_4 (57.6 μL, 1.02 mmol) in EtOH (1 mL) was added dropwise as N_2 evolved. The black suspension was stirred at room temperature for 15 min, heated under reflux for 10 min, cooled down, and then diluted with $CHCl_3$ (25 mL) in order to dissolve any organic product. The catalyst was removed by filtration through a Celite pad. Solvent removal gave crystalline 3,5-diferrocenylaniline (**2**), which was used without any further purification. Yield: 96%. ^{1}H NMR ($CDCl_3$): δ 3.6 (1.6 H, broad), 4.07 (10 H, s), 4.30 (4 H, d, $J = 1.6$ Hz), 4.63 (4 H, t, $J = 1.5$ Hz), 6.67 (2 H, d, $J = 1.25$ Hz), 7.06 (1 H, s). Mass spectrum (EI): $m/z = 461$ (100, M). Anal. Calcd for $C_{26}H_{23}Fe_2N$: C, 67.68; H, 4.99; N, 3.04. Found: C, 67.65; H, 4.76; N, 2.86.

(3,5-Diferrocenylphenyl)trimethylammonium Hexafluorophosphate (7). A stirred suspension of 3,5-diferrocenylaniline (**2**) (100 mg, 0.217 mmol), powdered sodium carbonate (70 mg, 0.651 mmol), and methyl iodide (81 μL, 13 mmol) in a mixture of CH_3CN (3 mL) and CH_3OH (3 mL) in a Schlenk tube was heated to reflux for 2 days. Then, more methyl iodide was added (81 μL, 13 mmol), and heating was continued for 6 days. After cooling, solvents were removed and an orange solid was extracted with hot CH_3CN (50 mL). To this solution was added potassium hexafluorophosphate (119.8 mg, 0.651 mmol), and the product was precipitated by addition of H_2O (200 mL) and filtered off on a glass frit. The solid was dried under vacuum with P_2O_5 and used without any further purification. Yield: 92%. ^{1}H NMR (CD_3CN): δ 3.58 (9 H, s), 4.13 (10 H, s), 4.48 (4 H, s), 4.95 (4 H, s), 7.54 (2 H, s), 7.79 (1 H, s). Mass spectrum (FAB) $m/z = 504$ (100, M^+).

X-ray Structure Determinations of Compounds 1o, 3, and 5. Single crystals of **1o**, **3**, and **5** were grown by vapor diffusion (dichloromethane/diethyl ether). Diffraction data were collected at 24 °C on an Enraf-Nonius CAD-4 diffractometer, using graphite-monochromated Mo Kα radiation ($\lambda = 0.710\ 69$ Å, $\omega-2\theta$ scanning mode). Lattice parameters and orientation matrices were determined by least-squares analysis of the 2θ angles of 25 reflections. The structures were solved by direct methods (SIR92)[44] and successive Fourier syntheses and refined by full (for **1o** and **3**) or block (for **5**) matrix least-squares refinements on σF^2 with the CRYSTALS program.[45] For **3** and **5**, the data were not corrected for absorption, but for **1o**, an absorption correction was carried out using the DIFABS[46] program. For **3** and **5**, unit weights were used throughout. For **1o**, in the final stages of the refinement, to each reflection was assigned a weight calculated from a Chebyshev[47] series with three coefficients (5.06, −1.02, and 3.87). Non-hydrogen atoms were refined with anisotropic displacement factors. Hydrogen atoms were placed geometrically (d(C−H) = 0.98 Å, fixed temperature factors = 0.06 Å^2), their positions being recalculated after refinement cycle. Neutral atom scattering factors and their anomalous dispersion corrections were taken from the *International Tables for X-ray Crystallography*.[48] Illustrations were obtained with the CAMERON package;[49] all calculations were performed on an IPC Pentium 100. Crystallographic data and the parameters of structure refinements are given in Table 1. Selected bond lengths and torsion angles are given in Table 2.

Molecular Orbital and V_{ab} Calculations. Molecular orbitals were calculated at the extended Hückel level for symmetrized planar geometries using the CACAO program,[50] which allows an easy visualization of the orbitals. Iron parameters were as follows: exp4s = 1.58; coul4s = −9.1; exp4p = 0.98; coul4p = −5.32; exp3d1 = 5.35; coul3d = −11.46; c1 = 0.53659; c2 = 0.66779; exp3d2 = 1.8. From molecular orbital calculations, V_{ab} couplings were determined as described elsewhere[35] from the splitting between orbitals with high weights on the metal atoms and opposite symmetries.

Acknowledgment. D. de Montauzon is gratefully acknowledged for precious advice about differential pulse voltammetry and the construction of a microelectrolysis cell. O. Riant is also aknowledged for fruitful discussions about palladium-catalyzed ferrocene arylation. Thanks are also gratefully expressed to G. Balacco (Menarini Industrie) for a copy of SwaN-MR and to J. Bonvoisin for the pulsed differential voltammetry simulation program.

Appendix. Calculations of $|g_b(t)|^2$ for Selected Systems

The calculation of $|g_b(t)|^2$ can be done analytically by solving directly the time-dependent Schrödinger equation for a limited number of n-state systems. In the case of the three-state system

(44) Altomare, A.; Cascarano, G.; Giacovazzo, G.; Guagliardi, A.; Burla, M. C.; Polidori, G.; Camalli, M. SIR92, A Program for Automatic Solution of Crystal Structure by Direct Methods. *J. Appl. Crystallogr.* **1994**, *27*, 435−435.
(45) Watkin, D. J.; Prout, C. K.; Carruthers, R. J.; Betteridge, P. *CRYSTALS. Issue 10*; Chemical Crystallography Laboratory, Univ. of Oxford: Oxford, UK, 1996.
(46) Walker, N.; Stuart, D. *Acta Crystallogr.* **1983**, A*39*, 158−166.
(47) Carruthers, J. R.; Watkin, D. J. *Acta Crystallogr.* **1979**, *A35*, 698−699.
(48) *International Tables for X-Ray Crystallography;* Kynoch: Birmingham, England, 1974; Vol. IV.
(49) Watkin, D. J.; Prout, C. K.; Pearce, L. J. *CAMERON*; Chemical Crystallography Laboratory, Univ. of Oxford: Oxford, UK, 1996.
(50) CACAO PC Version 4.0, July 1994. Mealli, C.; Proserpio, D. M. *J. Chem. Educ.* **1990**, *67*, 399−402.

presented in Figure 11, this solution can be written

$$|g_b(t)|^2 = 2\beta^2\gamma^2(\beta^2+\gamma^2)^{-1}[1-\cos(\omega_1 t)\cos(\omega_2 t) + A_1\sin(\omega_1 t)\sin(\omega_2 t) - A_2\sin^2(\omega_2 t)]$$

with, for the amplitudes,

$$A_1 = \Delta E[\Delta E^2 + 4(\beta^2+\gamma^2)]^{-1/2} \quad \text{and} \quad A_2 = 2(\beta^2+\gamma^2)[\Delta E^2 + 4(\beta^2+\gamma^2)]^{-1}$$

and, for the frequencies (with $\hbar = 1$),

$$\omega_1 = \Delta E/2 \quad \text{and} \quad \omega_2 = 0.5[\Delta E^2 + 4(\beta^2+\gamma^2)]^{1/2}$$

One example of the time evolution of a three-state system using this solution is provided in Figure 12a for a specific selection of the controlling parameters (β, γ, ΔE).

For the four-state system, Figure 11, analytical solutions can be obtained in a limited number of cases. For example, for $\Delta E_2 = \Delta E_3 = \Delta E$ and $\gamma = \beta$, this solution is given by

$$|g_b(t)|^2 = 2(\beta^2+\beta\delta)^2(X_1-X_2)^{-2}[1 + A_1(1-2A_1)^{-1}\times \sin^2(\omega_1 t) + A_2(1-2A_2)^{-1}\sin^2(\omega_2 t) - \cos(\omega_1 t)\cos(\omega_2 t) - (1-2A_1)^{-1/2}(1-2A_2)^{-1/2}\sin(\omega_1 t)\sin(\omega_2 t)]$$

with, for the amplitudes,

$$A_1 = X_1\Delta E^{-2} \quad \text{and} \quad A_2 = X_2\Delta E^{-2}$$

$$X_1 = -(3\beta^2+\delta^2) + ((3\beta^2+\delta^2)^2 - 4\beta^2(\beta-\delta)^2)^{1/2}$$

$$X_2 = -(3\beta^2+\delta^2) - ((3\beta^2+\delta^2)^2 - 4\beta^2(\beta-\delta)^2)^{1/2}$$

and, for the frequencies (with $\hbar = 1$),

$$\omega_1 = (\Delta E/2)(1-2A_1)^{1/2} \quad \text{and} \quad \omega_2 = (\Delta E/2)(1-2A_2)^{1/2}$$

The time evolution presented in Figure 12b corresponds to a four-state system with a selection of controlling parameters (β, γ, δ, ΔE_2, ΔE_3) demanding a calculation of the solution via the computed diagonalization of the corresponding Hamiltonian.

Supporting Information Available: A figure depicting the second molecule in the asymmetric unit of compound **5** (1 page). Three X-ray crystallographic files, in CIF format, are available on the Internet only. Ordering and access information is given on any current masthead page.

IC970013M